International Journal of Heat and Mass Transfer 143 (2019) 118594

Contents lists available at ScienceDirect

International Journal of Heat and Mass Transfer

journal homepage: www.elsevier.com/locate/ijhmt

Enhancement of non-uniform magnetic field on saturated film boiling of magnetic nanofluid (MNF)

Kaikai Guo [a], Huixiong Li [a,*], Yuan Feng [a], Tai Wang [b], Jianfu Zhao [c,d]

[a] State Key Laboratory of Multiphase Flow in Power Engineering, Xi'an Jiaotong University, Xi'an 710049, PR China
[b] School of Energy Power and Mechanical Engineering, North China Electric Power University, Baoding 071003, PR China
[c] CAS Key Laboratory of Microgravity, Institute of Mechanics, Chinese Academy of Sciences (CAS), Beijing 100190, PR China
[d] School of Engineering Science, University of Chinese Academy of Sciences, Beijing 100190, PR China

ARTICLE INFO

Article history:
Received 26 March 2019
Received in revised form 14 August 2019
Accepted 15 August 2019
Available online 22 August 2019

Keywords:
Magnetic nanofluid (MNF)
Non-uniform magnetic field
Enhanced heat transfer
Film boiling

ABSTRACT

Previous studies pointed to the possibility of controlling magnetic nanofluid (MNF) boiling heat transfer by a magnetic field. In this study, the numerical model for the film boiling of the MNF was developed to explore the heat transfer and dynamics characteristics of MNF film boiling under the non-uniform magnetic field. Due to the existence of magnetic field intensity gradient, the dynamics of the separated bubbles in the non-uniform magnetic field was different from that in the uniform magnetic field. First, the single-mode film boiling was performed to study the dynamics of the separated bubble in detail. As the magnetic field intensity increased, the magnetic field force in the vertical direction increased, causing the bubble to escape and rise faster. Due to the non-uniformity of the magnetic field in the vertical and horizontal directions, the results of multi-mode film boiling influenced by the non-uniform magnetic field were different from those of single-mode film boiling. As a result of the horizontal component of the magnetic field force, the instability wavelength of film boiling became shorter and the bubble formation sites on the heated wall gradually deviated towards the central axis during the bubble generation stage. As the magnetic field intensity increased, the deviation of the bubble increased due to the increasing horizontal component of the magnetic field force. More importantly, the heat transfer performance of a MNF with a non-uniform magnetic field applied in this paper was enhanced with a higher magnetic field intensity. The enhancement effect is more pronounced in the film boiling for water near the critical pressure.

1. Introduction

Energy is the basis of human survival and development. The world's mineral resources are limited and the environment has deteriorated in recent years. Therefore, saving energy and improving energy efficiency are important measures to ease the energy shortage. Enhancing heat transfer is an effective method for saving energy. There are many ways to enhance heat transfer, of which boiling heat transfer is an important field. Due to its high heat transfer coefficient, boiling heat transfer has been widely applied in many engineering fields, such as nuclear energy construction, thermal engineering, refrigeration industry, chemical engineering, etc. In order to further improve the heat transfer efficiency and safety performance of the thermal device, the related studies on enhancing boiling heat transfer are greatly necessary.

Over the decades, many ways have been developed to enhance boiling heat transfer. Among them, it is also an idea to seek a working medium with better performance and easier to achieve enhanced heat transfer. Many researchers have carried out a lot of experimental and numerical researches to study boiling heat transfer performance of various fluid media. Different heat transfer fluids exhibit different heat transfer performance due to their different physical properties. As a new type of intelligent fluid, the magnetic nanofluid (MNF) has been increasingly favoured by many scholars due to its unique advantages. MNFs, which consist of colloidal mixtures of nanoparticles coated with a surfactant and suspended within a nonmagnetic base fluid, constitute a special nanofluid that exhibit both magnetic properties of solid magnetism and fluid fluidity [1]. In the absence of gravity and magnetic field, MNFs have good stability and will not appear aggregation and deposition. Therefore, MNFs have a broad application prospect and are considered as the most promising and intelligent material in the field of material science [2]. Because of its higher effective

* Corresponding author.
E-mail address: huixiong@mail.xjtu.edu.cn (H. Li).

https://doi.org/10.1016/j.ijheatmasstransfer.2019.118594
0017-9310/

thermal conductivity and heat transfer characteristic controlled by external magnetic field, MNFs have a great application prospect in thermal engineering field [2,3]. In recent years, Great progress has been made in the experimental study of the boiling heat transfer mechanism of MNFs [4–21]. Such a consensus has been reached that the related studies on MNF boiling issues are very interesting and important for implementing the foundational studies on the hydrodynamics of MNFs and promoting practical engineering applications of MNFs. Previous studies pointed to the possibility of controlling magnetic boiling heat transfer by a magnetic field.

Considering the difficulty of MNF boiling issues, the numerical methods have been applied by more and more scholars to study MNF boiling heat transfer. The pool boiling heat transfer of a MNF under a non-uniform magnetic field was investigated numerically in a two-dimensional (2D) rectangular domain by Karimi-Moghaddam et al. [22]. In their studies, the boiling curves with and without magnetic field were presented and the performance of boiling heat transfer was enhanced significantly when using a MNF under a magnetic field. A numerical model with the two fluid model was applied by Mohammadpourfard et al. [23–25] to simulation the heat transfer performance of MNFs in the pool boiling and flow boiling. MNFs own higher heat transfer performance than pure liquids, and the heat transfer can be further enhanced under a non-uniform magnetic field. Malvandi et al. [26] analyzed theoretically the MNF film boiling on vertical plates and then simulated numerically the effects of various factors (e.g. the size of nanoparticles, the volume concentration, and the direction of magnetic field) on heat transfer under uniform magnetic fields. MNF boiling issues with a magnetic field were studied numerically with a molecular dynamics method (MD) by Taheri and Mohammadpourfard [27]. In their study, MNFs containing hydrophobic nanoparticles are more prone to film boiling.

Although the research and application of the MNFs have been experienced in decades, mechanisms of the effect of magnetic field on the MNF boiling have not been fully understood. In addition, in previous studies, few studies have been conducted on the motion characteristics of boiling bubbles in MNFs. Furthermore, the motion characteristics of MNF boiling bubbles under the non-uniform magnetic field have not been reported in published literatures. For the past few years, the various numerical methods of two-phase flow of MNFs have been proposed by more and more scholars [28–30]; thus, great progress in the method make it possible to numerically simulate the motion characteristics of boiling bubbles in MNFs. A numerical model to simulation the film boiling of a MNF with magnetic actuation under the uniform magnetic field was proposed in our previous study [31]. Effects of some key parameters, including volume concentration of nanoparticles, magnetic field intensity and magnetic susceptibility, on the heat transfer and dynamics characteristics of MNF film boiling were studied in detail. However, the motion characteristics of bubbles under the uniform magnetic field is different significantly from that under the non-uniform magnetic field. The related studies in MNF film boiling in presence of a non-uniform magnetic field is very necessary for enhancing further boiling heat transfer and promoting the further development and application of MNFs.

2. Numerical modelling

2.1. Interface tracking

In this study, the VOSET method [32], a coupled volume-of fluid and level set method, was used to capture the interface. The parameter c represents the VOF function, which varies between 0 and 1, which can be calculated by the following VOF equation:

$$\frac{\partial c}{\partial t} + \boldsymbol{u} \cdot \nabla c = 0 \tag{1}$$

For more details on the implementation of the VOSET method, please refer to literatures [32,33]. The density ρ, viscosity η and magnetic permeability μ can be calculated by the following expressions:

$$\rho(\phi) = \rho_g H(\phi) + \rho_l(1 - H(\phi)) \tag{2}$$

$$\eta(\phi) = \eta_g H(\phi) + \eta_l(1 - H(\phi)) \tag{3}$$

$$\mu(\phi) = \mu_g H(\phi) + \mu_l(1 - H(\phi)) \tag{4}$$

where ϕ is the level set function. $H(\phi)$ is the smooth Heaviside function and can be expressed as:

$$H(\phi) = \begin{cases} 0 & \text{when } \phi < -s \\ \frac{1}{2}\left[1 + \frac{\phi}{s} + \frac{1}{\pi}\sin\left(\frac{\pi\phi}{s}\right)\right] & \text{when } |\phi| < s \\ 1 & \text{when } \phi > s \end{cases} \tag{5}$$

where s is the width of transition region for smoothing, which equals to 1.5 h. h is the grid size.

2.2. Governing equations

For the viscous and incompressible two-phase boiling problems, the governing equations can be written as:

$$\nabla \cdot \boldsymbol{u} = \dot{m}\left(\frac{1}{\rho_g} - \frac{1}{\rho_l}\right) \tag{6}$$

$$\rho\left(\frac{\partial \boldsymbol{u}}{\partial t} + \boldsymbol{u} \cdot \nabla \boldsymbol{u}\right) = -\nabla p + \nabla \cdot \left[\eta\left((\nabla \boldsymbol{u}) + (\nabla \boldsymbol{u})^{\mathrm{T}}\right)\right] + \rho \boldsymbol{g}(1 - \beta_T(T - T_{sat})) + \boldsymbol{f}_s + \boldsymbol{f}_m \tag{7}$$

$$\frac{\partial T}{\partial t} + \boldsymbol{u} \cdot \nabla T = \frac{k}{\rho C_p}\nabla^2 T \tag{8}$$

$$\frac{\partial c}{\partial t} + \boldsymbol{u} \cdot \nabla c = \frac{\dot{m}}{\rho_g} \tag{9}$$

$$\nabla \cdot (\mu \nabla \psi) = 0 \tag{10}$$

where $\dot{m}$ refers to the mass transfer rate which means the magnitude of mass transfer per time in a cell. $\boldsymbol{f}_s$ is the surface tension. $\boldsymbol{f}_m$ is the magnetic force. Introducing the magnetic scalar potential ψ defined by $\boldsymbol{H} = -\nabla\psi$, the magnetic field intensity $\boldsymbol{H}$ is easily solved. μ is the relative permeability.

$\boldsymbol{f}_s$ is calculated using a CSF model [34] and expressed as

$$\boldsymbol{f}_s = -\sigma\kappa(\phi)\delta(\phi)\nabla\phi \tag{11}$$

where σ represents the surface tension coefficient. $\kappa(\phi)$ is the interface curvature. $\delta(\phi)$ is the Dirac delta function. $\kappa(\phi)$ and $\delta(\phi)$ are calculated as follows:

$$\kappa(\phi) = \nabla \cdot \left(\frac{\nabla\phi}{|\nabla\phi|}\right) \tag{12}$$

$$\delta(\phi) = \begin{cases} 0 & \text{when } |\phi| > s \\ \frac{1}{2s}\left[1 + \cos\left(\frac{\pi\phi}{s}\right)\right] & \text{when } |\phi| \leqslant s \end{cases} \tag{13}$$

For an isothermal and linearly magnetizable MNF, $\boldsymbol{f}_m$ can be given by Rosensweig [35], written as follows:

$$f_m = -\frac{1}{2}H^2\nabla\mu \tag{14}$$

Substituting Eq. (4) into Eq. (14), $\boldsymbol{f}_m$ can be further expressed as:

$$\boldsymbol{f}_m = -\frac{1}{2}H^2\left(\mu_l - \mu_g\right)\delta(\phi)\nabla\phi \tag{15}$$

In this study, the finite volume method was used to discretize the governing equations in the collocated grid system. QUICK and central difference schemes were used to discretize the convection and diffusion terms. In this paper, for an interfacial cell containing the phase interface, the temperature is estimated approximately by Ling et al.'s method [36].

The density, specific heat, thermal conductivity and viscosity of MNFs are calculated as follows [35]:

Density:

$$\rho_{mix} = (1-\varphi)\rho_l + \varphi\rho_p \tag{16}$$

Specific heat:

$$c_{p,mix} = \frac{(1-\varphi)\rho_l c_{p,l} + \varphi\rho_p c_{p,p}}{\rho_{mix}} \tag{17}$$

Thermal conductivity:

$$k_{mix} = \left(\frac{k_p + 2k_l - 2\varphi(k_l - k_p)}{k_p + 2k_l + \varphi(k_l - k_p)}\right)k_l \tag{18}$$

Dynamic viscosity:

$$\eta_{mix} = (1 + 2.5\varphi)\eta_l \tag{19}$$

where φ represents the volume concentration of nanoparticles.

In an interfacial cell with phase interface, the relationship of the mass transfer and heat flux should be expressed as:

$$\int_\Omega \dot{m}dV = \frac{1}{\gamma}\int_\Gamma \dot{q}dA \tag{20}$$

where γ is the latent heat of evaporation. dV is the volume of a cell. dA is the area of the phase interface. $\dot{q}$ is defined as:

$$\dot{q} = k_g\frac{\partial T}{\partial n}\Big|_g - k_l\frac{\partial T}{\partial n}\Big|_l \tag{21}$$

Combining Eqs. (20) and (21), the mass transfer mate can be calculated as follows:

$$\int_\Omega \dot{m}dV = \frac{1}{\gamma}\left(k_g\frac{\partial T}{\partial n}\Big|_g - k_l\frac{\partial T}{\partial n}\Big|_l\right)\Delta A \tag{22}$$

2.3. Physical properties and computational domain

The physical properties of the MNF mentioned in this paper are displayed in Table 1. The most dangerous wavelength of film boiling is $\lambda_0 = 2\pi\sqrt{3\sigma/\left(g\left(\rho_l - \rho_g\right)\right)}$ in 2-D. The schematic of the computational zone is shown in Fig. 1. A vertical upward non-uniform magnetic field is applied to the computational domain. The computational domain is on the same axis as the coil. As is well known, the magnetic field line is a set of parallel lines with the same direction and equal spacing in a uniform magnetic field. However, the magnetic field line produced by the coil is a set of closed curves in a non-uniform magnetic field, emitted from the upper surface of the coil and returned to the lower surface of the coil. Fig. 1 also gives the schematic of magnetic field line in the computational domain (The dotted line represents the magnetic field line). The magnetic field lines cross the boundary of the computational domain, so the component H_x and H_y of the magnetic field intensity $\boldsymbol{H}$ on the boundary are not zero. If we know the magnetic field intensity perpendicular to the boundary, we can solve the magnetic potential equation (10) of the non-uniform magnetic field by using the same treatment method as uniform magnetic field [31].

Table 1
Properties of the MNF.

	Liquid	Vapour	Nanoparticle
Density (kg/m^3)	200.0	5.0	5600.0
Thermal conductivity (W/m K)	40.0	1.0	6.0
Thermal capacity (J/kg K)	400.0	200	670.0
Dynamic viscosity (kg/m s)	0.1	0.005	
Surface tension coefficient (N/m)	0.1		
Latent heat (J/kg)	10000.0		
Magnetic susceptibility	0.2		

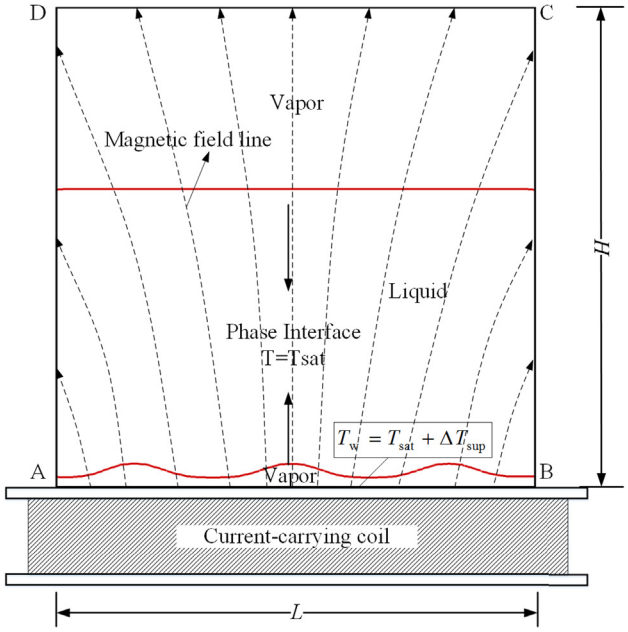

Fig. 1. Schematic of the computational domain. The dotted line represents the magnetic field line and the red line represents the phase interface. (For interpretation of the references to colour in this figure legend, the reader is referred to the web version of this article.)

2.4. Boundary conditions of flow field

For solving the flow field accurately, the boundary conditions in the computational domain are defined as:

At x = 0 and x = L,

$$u = 0,\ \frac{\partial v}{\partial x} = \frac{\partial T}{\partial x} = 0 \tag{23}$$

At y = H,

$$\frac{\partial u}{\partial y} = \frac{\partial v}{\partial y} = \frac{\partial T}{\partial y} = 0 \tag{24}$$

At y = 0,

$$u = v = 0,\ T_w = T_{sat} + \Delta T_{sup} \tag{25}$$

2.5. Boundary conditions of the non-uniform magnetic field

The method of constructing the boundary conditions of a non-uniform magnetic field, mentioned by Shi et al. [37], is introduced in this section. It is assumed that the magnetic field intensity on the central axis of the coil has only the components of y axis, and $H(y) = B_0 + B_1y + B_2y^2 + B_3y^3 + B_4y^4 + B_5y^5$. ψ represents the

magnetic potential in the absence of vapour. From $\boldsymbol{H} = -\nabla\psi$, we can see that on the central axis of the coil, ψ is the sixth polynomial in y, and $\psi(x_0, y) = P_6(y)$. Here, $x_0 = 0.5\ Lx$. $P_6(y)$ can be written as follows

$$P_6(y) = -\int H(y)dy = -\left(B_0 y + \frac{1}{2}B_1 y^2 + \frac{1}{3}B_2 y^3 + \frac{1}{4}B_3 y^4 + \frac{1}{5}B_4 y^5 + \frac{1}{6}B_5 y^6\right) \quad (26)$$

When there is no vapour, $\nabla\cdot(\nabla\psi) = 0$. For two-dimensional cartesian coordinates,

$$\frac{\partial^2\psi}{\partial^2 x} + \frac{\partial^2\psi}{\partial^2 y} = 0 \quad (27)$$

Since ψ is symmetrically distributed with respect to $x = x_0$, and $\psi(x_0, y) = P_6(y)$, the expression of ψ can be defined as

$$\psi(x,y) = P_6(y) + (x - x_0)^2 P_4(y) + (x - x_0)^4 P_2(y) + (x - x_0)^6 P_0(y) \quad (28)$$

where $P_4(y) = A\cdot P_6^{(2)}(y)$, $P_2(y) = B\cdot P_6^{(4)}(y)$, $P_0(y) = C\cdot P_6^{(6)}(y)$. Eq. (28) is substituted into Eq. (27), and the values of coefficients A, B and C are $-1/2$, $1/24$, $-25/756$, respectively. Therefore, the expressions of $P_4(y)$, $P_2(y)$ and $P_0(y)$ are shown as

$$\begin{aligned} P_4(y) &= -\tfrac{1}{2}P_6^{(2)}(y) = \tfrac{1}{2}\left(B_1 + 2B_2 y + 3B_3 y^2 + 4B_4 y^3 + 5B_5 y^4\right) \\ P_2(y) &= \tfrac{1}{24}P_6^{(4)}(y) = -\tfrac{1}{12}\left(3B_3 + 12B_4 y + 30B_5 y^2\right) \\ P_0(y) &= -\tfrac{25}{756}P_6^{(6)}(y) = \tfrac{1}{6}B_5 \end{aligned} \quad (29)$$

After Eq. (29) is substituted into Eq. (28) to obtain the whole magnetic potential $\psi(x, y)$, the magnetic field intensity component on the boundary of the computational domain can be calculated. And then the magnetic field value is taken as the magnetic field boundary condition of the non-uniform magnetic field. The processing method of the non-uniform magnetic field boundary condition is similar to the uniform magnetic field, and is processed by the additional source term method. Finally, the magnetic potential $\psi(x, y)$ in presence of vapour in the computational domain can be obtained. The accuracy of the magnetic field model with a uniform magnetic field had been verified in our previous study [31].

3. Numerical method validation

In the present study, a non-uniform magnetic field is established by the method which is described in Section 2.5. In order to verify the reasonability of the establishment of the non-uniform magnetic field, simulations have been performed in the domain size of $3\lambda_0 \times 3\lambda_0$. Here, the magnetic field intensity at $y = 0.04$ m is defined as H_0. The coefficients of B_0, B_1, B_2, B_3, B_4, and B_5 under different magnetic field intensity H_0 of 5 kA/m, 10 kA/m, 15 kA/m, 20 kA/m, 25 kA/m and 30 kA/m are shown in Table 2.

The distributions of magnetic field lines and magnetic field intensity calculated numerically by the magnetic field model in this paper are shown in Fig. 2. It can be seen in the figure that

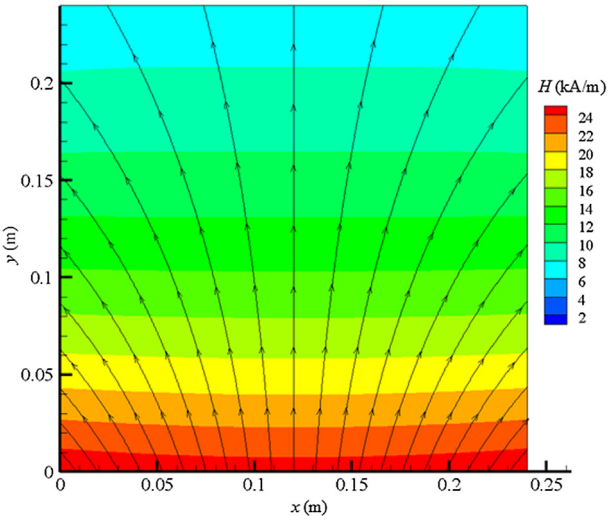

Fig. 2. Magnetic streamlines and magnetic field intensity when $H_0 = 20$ kA/m.

the magnetic field line is emitted from the bottom of the computational domain and has a divergent distribution. Furthermore, the magnetic field lines become sparser as a decrease in magnetic field intensity (i.e., away from the bottom boundary).

Fig. 3 gives the comparison of theoretical and numerical magnetic field intensity along the central axis of the computational domain. The solid line is the curve fitted with the fifth polynomial, which represents the theoretical magnetic field intensity along the central axis of the computational domain derived from the relation $H(y) = B_0 + B_1 y + B_2 y^2 + B_3 y^3 + B_4 y^4 + B_5 y^5$. And the discrete points in Fig. 3 show the numerical values of magnetic field intensity along the central axis of the computational domain. From the figure, it can be seen clearly that the numerical solution is consistent well with the theoretical value.

Next, there is no consideration of the volume concentration and magnetic field. The simulation has been performed in the domain size of $3\lambda_0 \times 3\lambda_0$. In order to check the grid independency, three different grid system including $\lambda_0/32$, $\lambda_0/64$ and $\lambda_0/128$ were used for this simulation. In this case, the wall superheat ΔT_{sup} equals to 2 K. The interfaces by different grid sizes at 0.45 s are shown in Fig. 4. The result shows that the interface has no significant change when the grid was finer than $\lambda_0/64$. Furthermore, the difference between the vapour volumes at $\lambda_0/64$ and $\lambda_0/128$ was less than 0.3%. Therefore, the $\lambda_0/64$ grid was used in the rest of our simulations.

The Nusselt number is defined as

$$Nu = \frac{1}{\lambda_0}\int_0^{\lambda_0} Nu' dx \quad (30)$$

where Nu' is the local Nusselt number, which is calculated as

$$Nu' = \frac{l_0}{T_w - T_{sat}}\left.\frac{\partial T}{\partial y}\right|_{y=0}, \text{ where } l_0 = \sqrt{\frac{\sigma}{(\rho_l - \rho_g)g}} \quad (31)$$

Table 2
The coefficients of the equation $H(y) = B_0 + B_1 y + B_2 y^2 + B_3 y^3 + B_4 y^4 + B_5 y^5$ under different gradient magnetic field.

Magnetic field intensity H_0 (kA/m)	B_0	B_1	B_2	B_3	B_4	B_5
5	6.181E + 03	−3.164E + 04	7.471E + 04	−9.505E + 04	6.207E + 04	−1.588E + 04
10	1.251E + 04	−7.306E + 04	2.162E + 05	−3.665E + 05	3.291E + 05	−1.197E + 05
15	1.838E + 04	−9.875E + 04	2.554E + 05	−3.658E + 05	2.745E + 05	−8.347E + 04
20	2.502E + 04	−1.398E + 05	3.854E + 05	−6.036E + 05	5.056E + 05	−1.746E + 05
25	3.089E + 04	−1.716E + 05	4.858E + 05	−8.019E + 05	7.163E + 05	−2.635E + 05
30	3.630E + 04	−1.541E + 05	2.150E + 05	5.783E + 04	−3.810E + 05	2.365E + 05

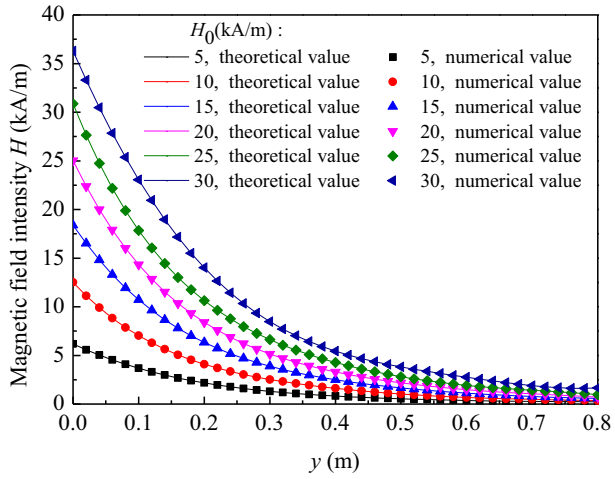

Fig. 3. The comparison of theoretical and numerical magnetic field intensity along the central axis of the computational domain.

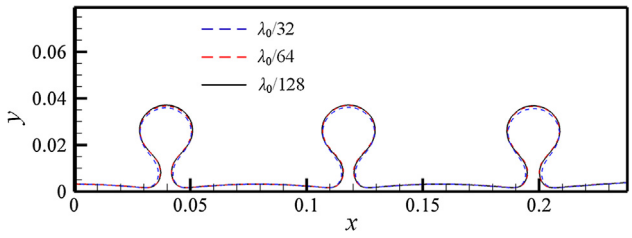

Fig. 4. The interface with different grid sizes at 0.45 s.

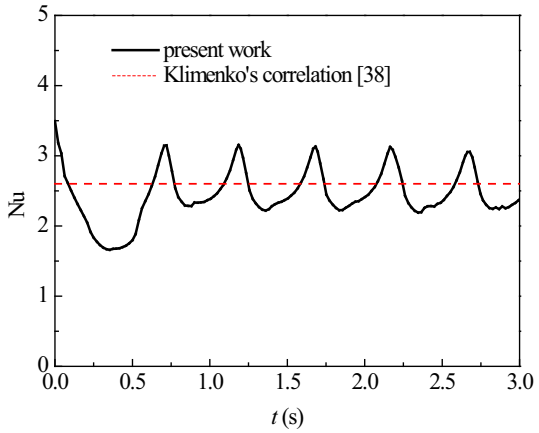

Fig. 5. The spatial average *Nu* number with time in validation case.

Klimenko's correlation [38] was used for validating the numerical method proposed in this study. Fig. 5 shows the Nu number with time. The space- and time- averaged Nu number calculated in this case is 2.49. The Nu number calculated from Klimenko's correlation is 2.6. The difference between them is 4.23%.

4. Results and discussion

4.1. Single-mode film boiling

First, in order to describe clearly and conveniently the motion mechanism of boiling bubble under a non-uniform magnetic field, the single-mode film boiling is performed in the computational domain of $\lambda_0 \times 3\lambda_0$. The dynamics of the first set of separated bubble are reported in detail in this section. Here, $\Delta T_{sup} = 2$ K, $\chi = 0.2$ and $\varphi = 0.1\%$. Fig. 6 displays the interface evolution separated bubble with the magnetic field. It can be seen in Fig. 6 that when the magnetic field is applied, the departure time and the departure diameter of separated bubbles are greatly reduced due to the existence of the magnetic field force. And, the larger the magnetic field intensity, the greater the magnetic field force acted on the bubble, leading to the increase in the departure time and the departure diameter, as shown in Fig. 7.

The influence of the magnetic field on the velocity field mainly reflects in the magnetic field force acted at the phase interface. The magnetic field force causes the disturbance and deformation of the phase interface and then the dynamic characteristics of the phase interface affects the velocity field nearby. The more detailed explanations are expounded below.

In the formation of the bubble, in our opinion, the main reason causing bubble to escape is that the phase interface is disturbed due to the presence of magnetic field so that the instability of phase interface become intense. And, with an increase in the magnetic field intensity, the instability effect becomes more intense. Consequently, the more intense the phase interface, the easier it is for the bubble to escape. Besides, based on our previous study [31], the magnetic field causes the most dangerous wavelength to decrease, and the stronger the magnetic field, the smaller the most dangerous wavelength. Obviously, the decrease of the most dangerous wavelength will reduce the bubble departure diameter.

After the detachment of the bubble, due to the non-uniformity of the magnetic field in the vertical directions, which is shown in Figs. 2 and 3, the magnetic force at the bottom of the bubble is greater than that at the top of the bubble. And the magnetic force acted on the phase interface directs towards the vapour phase. Therefore, the total magnetic force acted on the whole interface is positive in the direction of the y-axis so that the bubble is accelerated in the presence of the magnetic field. Fig. 8 plots the vertical velocity and magnetic field force distributions when the bubble detaches initially and rises steadily under different magnetic fields. It is shown in Fig. 8 that as the magnetic field intensity increases, the magnetic field force acted on the bubble increases and therefore the rise velocity increases due to the positive total magnetic field force. Besides, due to the driving effect of the non-uniform magnetic field on the bubble, the jet flow velocity of the liquid below the bubble increases.

Unlike the uniform magnetic field, the magnetic field intensity in the non-uniform magnetic field applied in this paper decreases gradually in the vertical direction. Due to the existence of magnetic field intensity gradient, the dynamics of the separated bubbles in the non-uniform magnetic field is different from that in the uniform magnetic field. Fig. 9 plots the vertical velocity curve of the bubble in the process of bubble formation, detachment and rise. Here, the bubble velocity is obtained by the displacement δs at the top of the bubble divided by the corresponding time interval δt. In Fig. 9, we can see that with the increase in magnetic field intensity, the bubble formation, detachment and rising velocity increase because of larger magnetic field force in vertical direction. After the detachment of the bubble, the other reason of the increase in bubble rising velocity is that the resistance of the bubble is reduced due to the decrease in the bubble departure diameter with the increase in the magnetic field intensity. The vertical component of the total magnetic field force is written as:

$$F_{mag,y} = \int_{\Omega} \boldsymbol{f}_m \cdot \boldsymbol{e}_y dV \tag{32}$$

Fig. 10 plots $F_{mag,y}$ versus the position of the rising bubble centre with different magnetic field intensities. As can be seen in Fig. 10, larger magnetic field intensity produces larger magnetic field force.

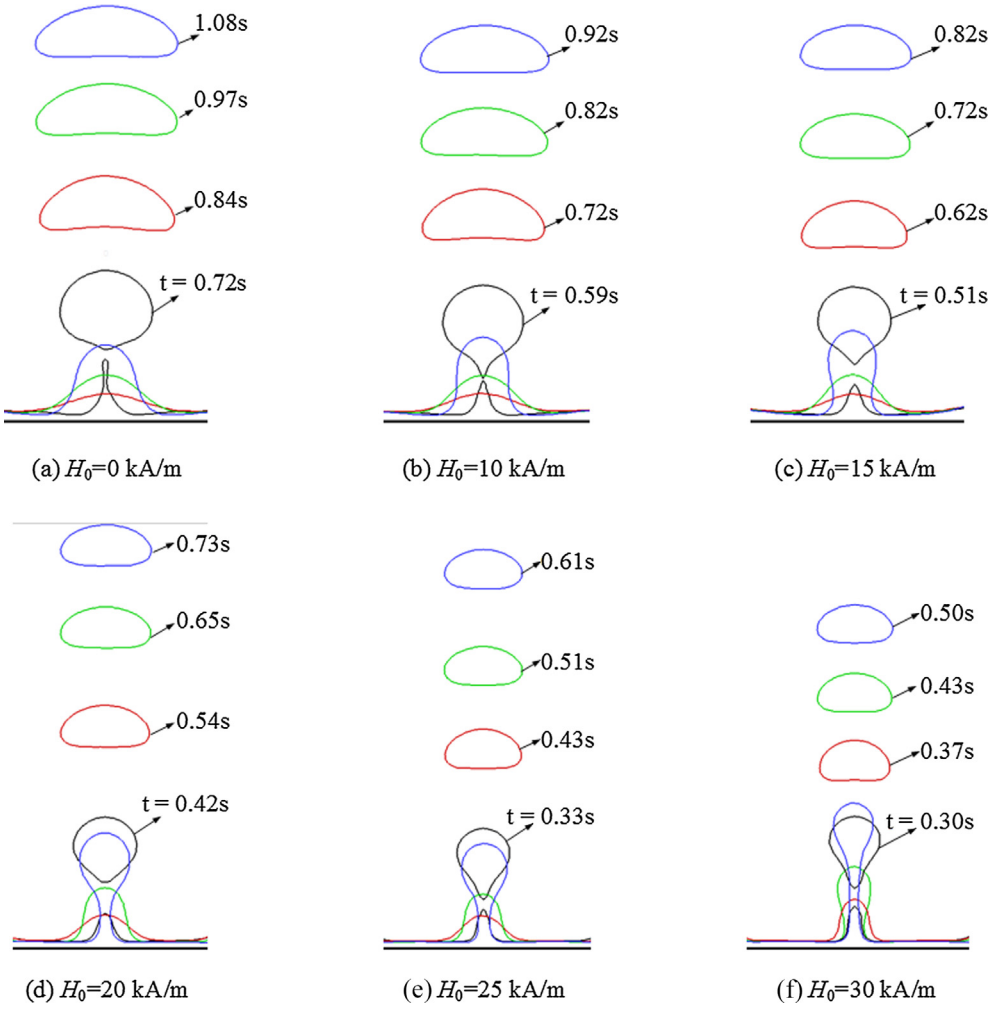

Fig. 6. Phase interface evolution of the first set of separated bubbles with different magnetic field intensities when ΔT_{sup} = 2 K. (a) H_0 = 0 kA/m; (b) H_0 = 10 kA/m; (c) H_0 = 15 kA/m; (d) H_0 = 20 kA/m; (e) H_0 = 25 kA/m; (f) H_0 = 30 kA/m.

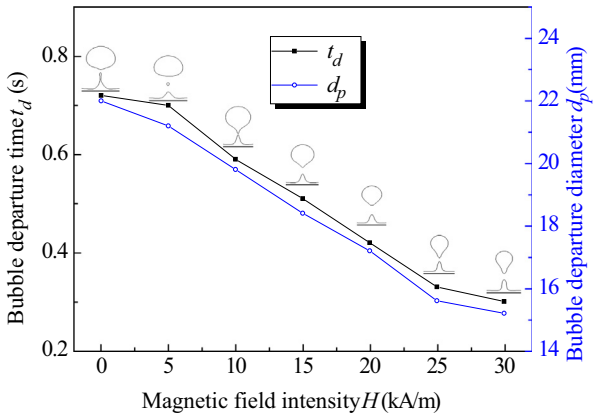

Fig. 7. Bubble departure time and bubble departure diameter for separated bubble with different magnetic field intensities.

And the magnetic field force gradually decreases with the rise of bubbles due to the decreasing negative magnetic field intensity gradient which is displayed in Fig. 3. Fig. 11 shows the typical evolution of bubble velocity field, velocity contour, and magnetic field intensity contours with different negative gradient magnetic fields. The results from Figs. 9 and 10 can be elucidated further in Fig. 11.

4.2. Multi-mode film boiling

The objective of this investigation is to reveal some light on multi-mode film boiling where the evolution of phase interface results in the formation of multiple bubbles. Under some certain conditions, the instability of the phase interface in multi-mode saturated film boiling is easy to occur. The instability becomes more intense when an external magnetic field is applied. In this study, we address the dynamics and heat transfer characteristics of multi-mode film boiling in presence of different non-uniform magnetic fields in the domain size of $3\lambda_0 \times 3\lambda_0$. Due to the non-uniformity of the magnetic field in the vertical and horizontal directions, which is shown in Fig. 2, the result of multi-mode film boiling influenced by the non-uniform magnetic field will be different from that of single-mode film boiling.

Fig. 12 displays the evolution of phase interface and velocity vector in multi-mode film boiling with different non-uniform magnetic fields. We can see in Fig. 12 that the bubble departure time and the bubble departure diameter both decrease with the increase in the magnetic field intensity. The result is consistent with that of single-mode film boiling.

If the magnetic field is absent, bubbles are detached periodically in the vertical direction and do not deviate in the horizontal direction, as shown in Fig. 12(a). However, after a non-uniform magnetic field is applied, the horizontal component of the magnetic

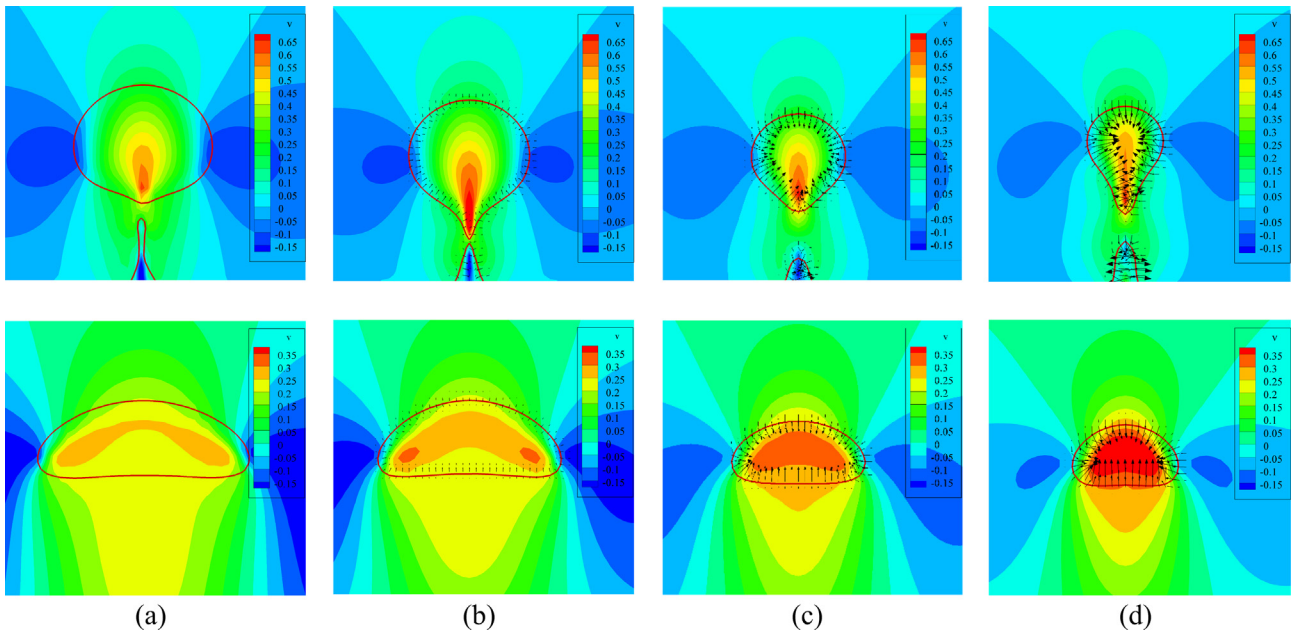

Fig. 8. The vertical velocity and magnetic field force distributions under different magnetic fields. The black solid lines with arrow represent the magnetic field force and the red lines represent the phase interface. (a) H_0 = 0 kA/m, (b) H_0 = 10 kA/m, (c) H_0 = 20 kA/m, (d) H_0 = 30 kA/m.

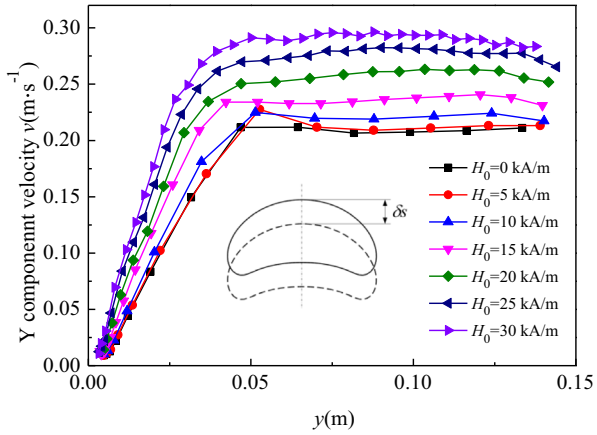

Fig. 9. Velocity variation of the bubble along the vertical direction from formation to departure with different magnetic field intensity.

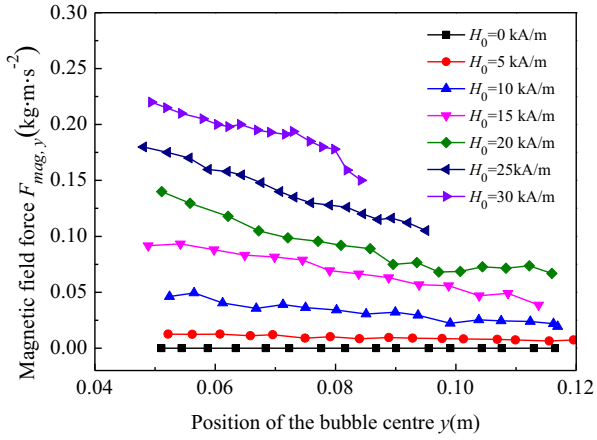

Fig. 10. Vertical component (F_{mag_y}) of the total magnetic field force versus the position of the rising bubble centre under different applied magnetic field intensities.

field force is not zero due to the existence of the magnetic field gradient in the horizontal direction. Therefore, the horizontal component of the magnetic field force will make a great influence on the process of bubble formation, detachment and rise in the non-uniform magnetic field. The bubble on the central axis is detached periodically because the horizontal component of the total magnetic force acted on the bubble cancels each other out. However, the horizontal component force of the total magnetic force acted on bubbles on both sides of a central axis are not zero, so the bubbles deviate in the horizontal direction.

When the magnetic field intensity is less than 5 kA/m, the horizontal component of the magnetic field force acted on the bubble is so small that the process of the bubble formation, detachment and rise are not influenced, as shown in Fig. 12(b). When the magnetic field intensity further changes from 5 kA/m to 20 kA/m, the flow field is homogeneous and is distributed symmetrically along the central axis. Besides, the detachment of the bubble still remains periodic. Taking H_0 = 20 kA/m as an example, the force analysis of the bubble in the formation process is expounded. Fig. 13 shows the horizontal component (H_x) of magnetic field intensity and distributions of magnetic field force acted on the bubble on the left side of the central axis at 0.64 s in presence of the non-uniform magnetic field of H_0 = 20 kA/m. According to the numerical results, it can be obtained that the horizontal component of magnetic field force acted on the bubble at the left side of the central axis is positive, while that acted on the bubble at the right side of the central axis is negative in the same way. The result indicates that the magnetic field force in the horizontal direction acted on the bubble on both sides of the central axis point to the central axis, so the bubble is offset to the central axis. In Fig. 12(c)–(e), it can be clearly seen that with an increase in the magnetic field intensity, the horizontal component of the total magnetic field force acted on the bubble on the heated wall increases during the process of bubble formation, leading to the gradual increase in the horizontal deviation of the bubble. In addition, it can be seen from Fig. 13 that the deviation at the bottom of the bubble is greater than that at the top of the bubble. This is because that the horizontal component of the magnetic field intensity (i.e. H_x) at the bottom of the bubble is greater than that at the

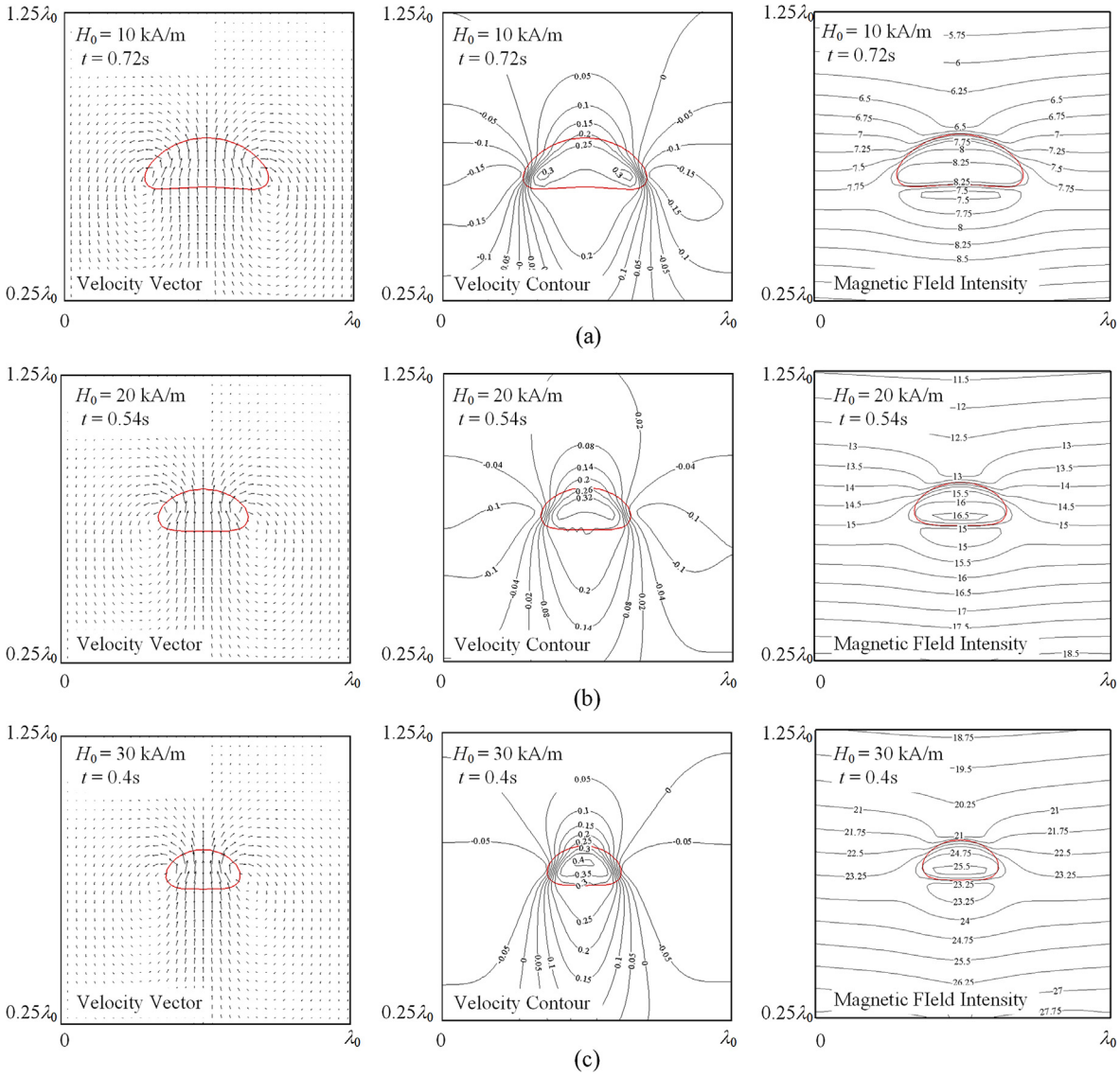

Fig. 11. Evolution of bubble velocity field, velocity contour, and magnetic field intensity contours with different H_0. (a) H_0 = 10 kA/m; (b) H_0 = 20 kA/m; (c) H_0 = 30 kA/m.

top of the bubble, so that the horizontal component of the magnetic field force at the bottom of the bubble is greater than that at the top of the bubble. In Fig. 14, the velocity vectors near the bubble on the left side of the central axis at 0.76 s are given when the magnetic field intensity H_0 is equal to 20 kA/m. In the process of the bubble rise, the non-uniform magnetic field causes a large disturbance in the flow field, and the distribution of the flow field is no longer symmetrical along the bubble, resulting in the dip angle between the jet flow at the bottom of the bubble and the vertical direction. Driven by the jet, the bubble rises towards the direction of the magnetic field line (the direction of the magnetic field line is shown in Fig. 2). When the magnetic field intensity is 25 kA/m, the bubble formation sites increases due to the stronger instability of phase interface. The stronger instability leads to larger disturbance of the flow field, resulting in the asymmetry of the flow field. The bubbles on the central axis are offset in the horizontal direction, and the formation and detachment of bubbles are no longer periodic. In the process of bubble formation and detachment, the bubble flow gradually evolved into the bubble column flow, as shown in Fig. 12(f).

Effects of different magnetic intensities on the heat transfer of MNF film boiling are displayed in Figs. 15 and 16. Fig. 15 plots the variation of the space-averaged Nusselt number over time under different magnetic field intensities. In Fig. 15, we can see that when the magnetic field intensity is less than 20 kA/m, the lines representing the space-averaged Nusselt number is periodic over time due to the bubbles detaching periodically from the heated surface. However, the bubble is detached randomly at the initial time and then the bubble morphology changes gradually after the magnetic field intensity further increases to 25 kA/m. The vapour column flow is formed. Therefore, the space-averaged Nusselt number is no longer periodic and unchanged basically over time. Fig. 15 gives Nusselt number and the enhancement ratio η. The enhancement ratio η can be calculated by the following equation:

$$\eta = \frac{\overline{Nu_M} - \overline{Nu_0}}{\overline{Nu_0}} \times 100\%$$

where $\overline{Nu_M}$ and $\overline{Nu_0}$ are Nusselt number with and without magnetic field, respectively. Here, the parameter η represents the ability of magnetic field to enhance heat transfer. In Fig. 16, it can be seen clearly that as the magnetic field intensity increases, the performance of heat transfer of a MNF in presence of the non-uniform magnetic field is enhanced. Furthermore, the magnetic field is so small that there is a negligible impact on heat transfer. For example,

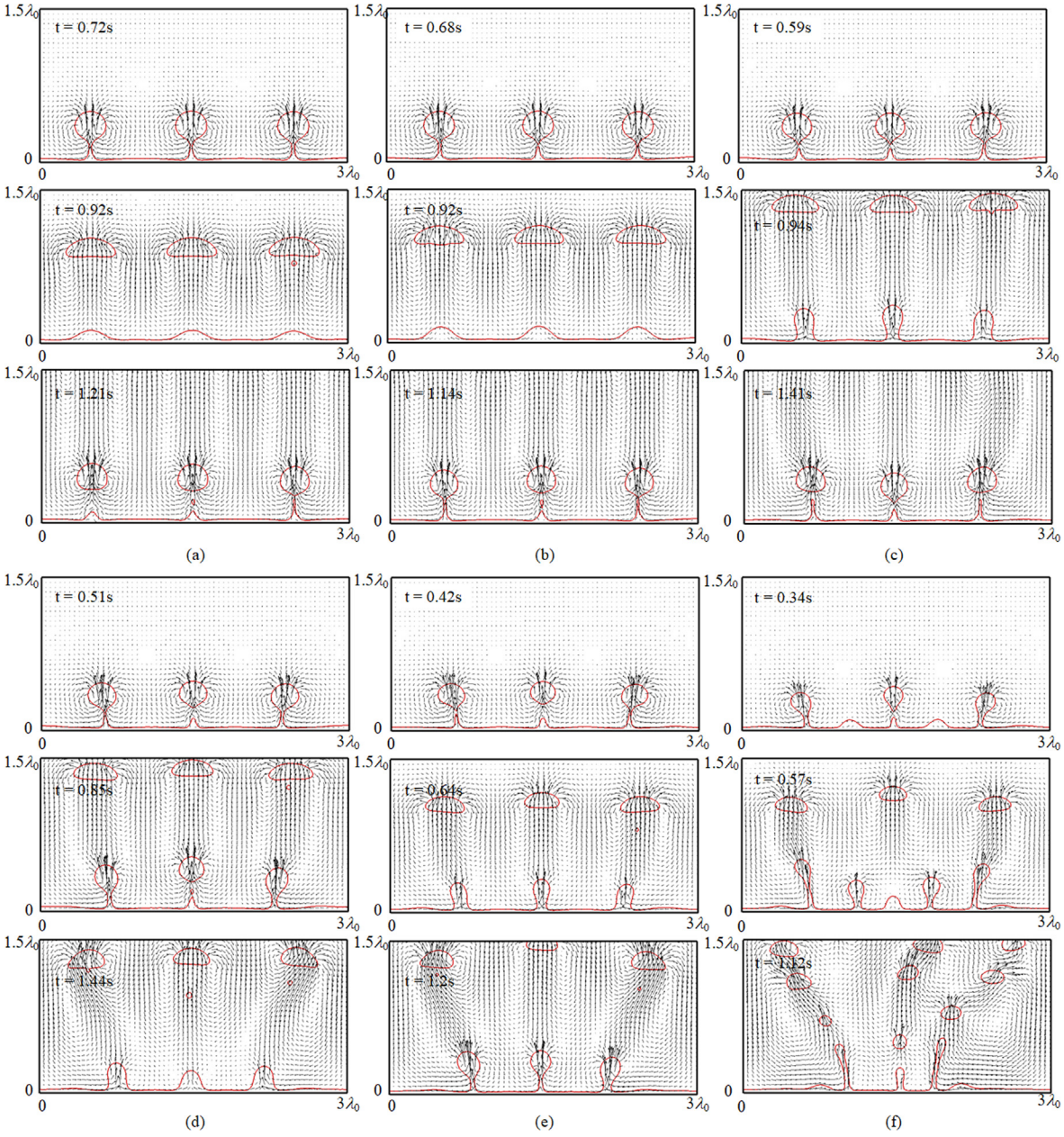

Fig. 12. Interface evolution and velocity vector under different non-uniform magnetic fields. (a) H_0 = 0 kA/m; (b) H_0 = 5 kA/m; (c) H_0 = 10 kA/m; (d) H_0 = 15 kA/m; (e) H_0 = 20 kA/m; (f) H_0 = 25 kA/m.

when the magnetic field intensity is equal to 5 kA/m, the enhancement ratio η is 1.1%. However, there is a significant effect on heat transfer under high magnetic field intensity. When the magnetic field intensity is 30 kA/m, the heat transfer can be enhanced up to 20%.

4.3. Film boiling for water near the critical pressure

In order to further confirm the reasonability and accuracy of the results in this paper, similar analysis has been performed for water near the critical pressure (21.9 MPa). The physical properties used are given in Table 3. The properties of magnetic nanoparticles are shown in Table 1. In this study, the magnetic susceptibility is set to 0.2. The wall superheat is 10 K. After checking the grid independency, the grid dimension is taken as $\lambda_0/240$ in all simulations performed in the computational domain of $\lambda_0 \times 3\lambda_0$, where the most dangerous wavelength λ_0 is 0.002275 m. The computational setup about the non-uniform magnetic field in this section is same to that in Section 4.1. The coefficients of B_0, B_1, B_2, B_3, B_4, and B_5 under different magnetic field intensity H_0 of 5 kA/m, 7.5 kA/m and 10 kA/m are shown in Table 4.

Fig. 17 plots the comparison of the interface morphology at the instant of the first set of the released bubble with different magnetic fields. In Section 4.1, the interface morphology without the magnetic field and with a non-uniform magnetic field of 5 kA/m is almost the same. However, we can obviously see in Fig. 17 that when a non-uniform magnetic field of 5 kA/m is applied, the interface morphology has changed dramatically. Obviously, the magnetic field has a greater influence on the film boiling for water near the critical pressure. The magnetic Bond number $\mathrm{Bo}_m = \mu_0 L H^2/\sigma$, which represents the influence of magnetic field and is the ratio of the magnetic force and the surface tension force,

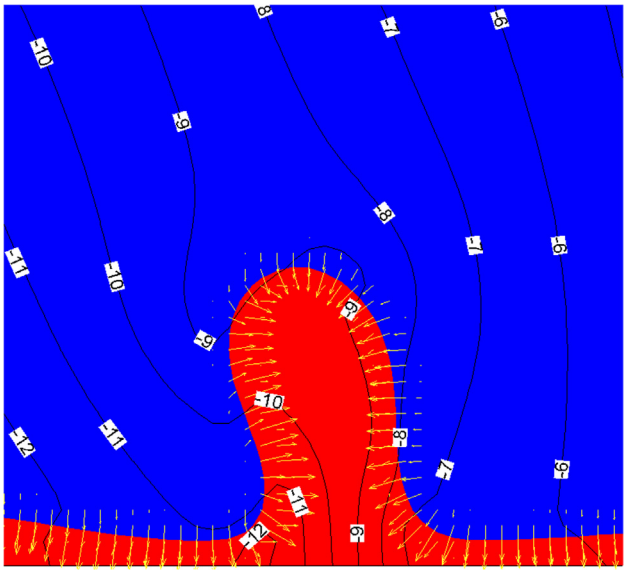

Fig. 13. Distributions of magnetic field force and horizontal component (H_x) of magnetic field intensity at 0.64 s in presence of the non-uniform magnetic field of H_0 = 20 kA/m. The black solid lines represent the contour of H_x and the yellow arrowed lines represent magnetic field force. (For interpretation of the references to colour in this figure legend, the reader is referred to the web version of this article.)

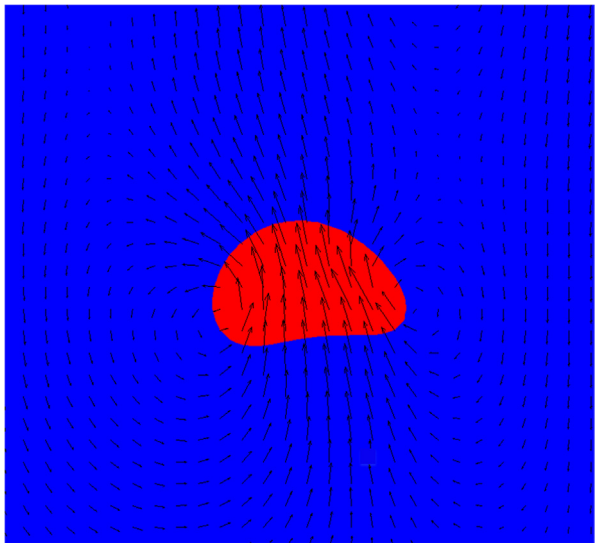

Fig. 14. velocity vector near the bubble on the left side of the central axis at 0.76 s is given when H_0 = 20 kA/m.

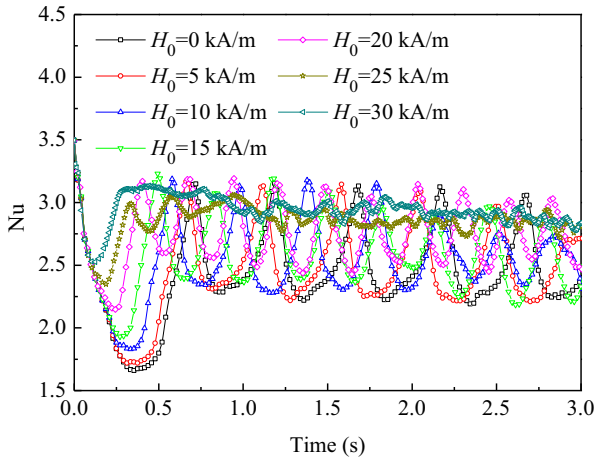

Fig. 15. Variation of space-averaged Nusselt number over time in presence of different non-uniform magnetic field.

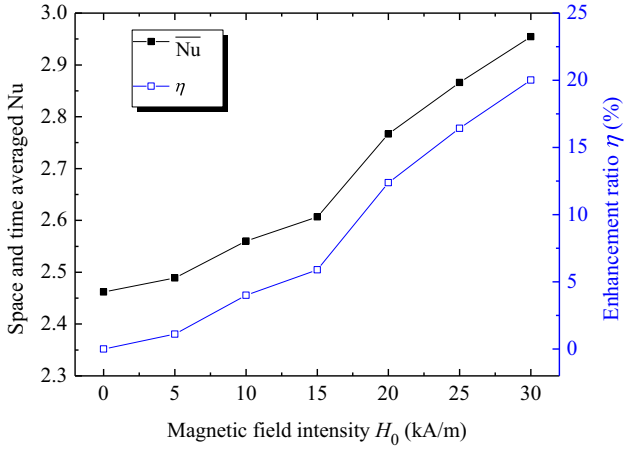

Fig. 16. Space- and time- averaged Nusselt number and the enhancement ratio η with different magnetic field intensities in presence of the non-uniform magnetic field.

Table 3
The physical properties of water near the critical pressure.

	Liquid	Vapour
Density (kg/m^3)	402.4	242.7
Thermal conductivity (W/m K)	0.5454	0.5383
Thermal capacity (J/kg K)	2.18×10^5	3.52×10^5
Dynamic viscosity (kg/m s)	4.67×10^{-5}	3.52×10^{-5}
Surface tension coefficient (N/m)	7.0×10^{-5}	
Latent heat (J/kg)	2.764×10^5	

is used to explain the phenomenon. In Section 4.1, when a magnetic field of 5 kA/m is applied, Bo_m= 2.27. However, for the water near the critical pressure with a magnetic field of 5 kA/m, Bo_m = 94.9, the magnetic force plays an absolutely dominant role. With an increase in magnetic field intensity, the interface morphology becomes more intense and the bubble departure diameter and the bubble departure time both sharply decrease. This conclusion is basically consistent with that of Section 4.1. The greater magnetic field intensity, the more intense the interface instability, and the more bubbles are generated. At the fixed computational domain, the numbers of bubble formation sites for the cases of H_0 = 0 kA/m, H_0 = 5 kA/m, H_0 = 7.5 kA/m and H_0 = 10 kA/m is one, three, five and eight. Fig. 18 also displays the interface evolution at the instant of the first set of the released bubble under the magnetic field intensity of H_0 = 5 kA/m. The figure indicates that during bubble growth, the bubble formation sites on the left and right sides of the central axis gradually move toward the central axis due to the non-uniformity of the magnetic field. The detailed explanation on the phenomenon has been discussed in Section 4.2.

Fig. 19 gives the effect of the non-uniform magnetic field on the heat transfer performance of film boiling for water near the critical pressure. The space- and time- averaged Nusselt number obtained from the computational results without the magnetic field is 4.03, and that predicted from Klimenko's correlation [38] is 4.20. The deviation is about 4%. So, the numerical result agree well with the correlation, which verifies the accuracy and reasonability of the present results.

Table 4
The coefficients of the equation $H(y) = B_0 + B_1y + B_2y^2 + B_3y^3 + B_4y^4 + B_5y^5$ under different gradient magnetic field applied in the film boiling for water near the critical pressure.

Magnetic field intensity H_0 (kA/m)	B_0	B_1	B_2	B_3	B_4	B_5
5	6.181E + 03	−3.164E + 06	7.471E + 08	−9.505E + 10	6.207E + 12	−1.588E + 14
7.5	9.403E + 03	−5.371E + 06	1.547E + 09	−2.567E + 11	2.275E + 13	−8.211E + 14
10	1.251E + 04	−7.306E + 06	2.162E + 09	−3.665E + 11	3.290E + 13	−1.200E + 15

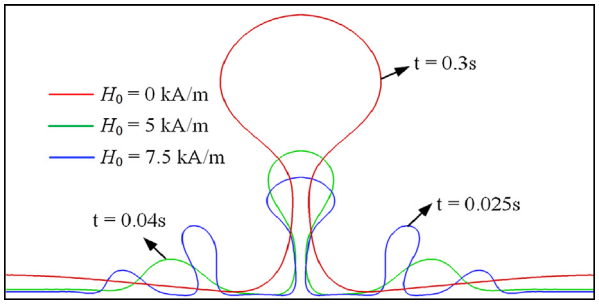

Fig. 17. Comparison of the interface morphology at the instant of the first set of the released bubble with different magnetic fields.

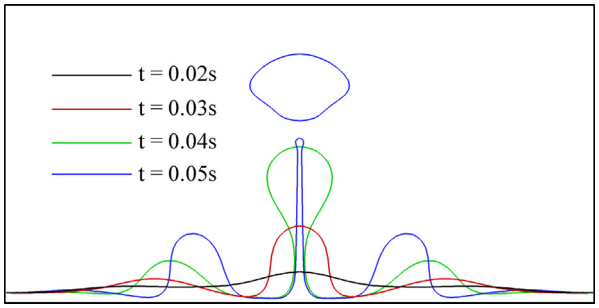

Fig. 18. Interface evolution at the instant of the first set of the released bubble under the magnetic field intensity of H_0 = 5 kA/m.

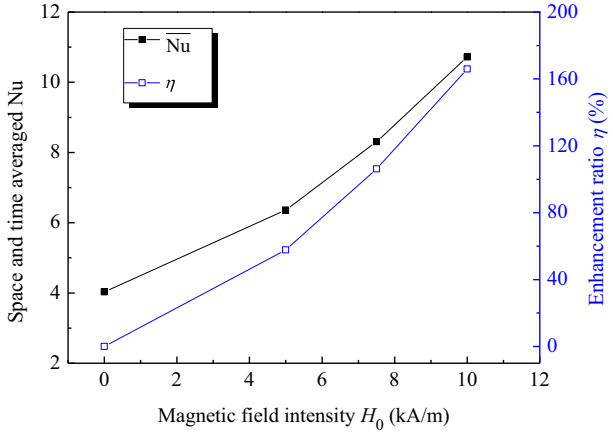

Fig. 19. Space- and time- averaged Nusselt number and the enhancement ratio η with different magnetic field intensities.

The space- and time- averaged Nusselt number and the enhancement ratio η under different magnetic field intensities are shown in Fig. 19. When the magnetic field of H_0 = 5 kA/m, H_0 = 7.5 kA/m or H_0 = 10 kA/m is applied, the enhancement ratio η is 58%, 106.2% or 166%, respectively. It is obvious that the heat transfer performance of film boiling for water near the critical pressure is greatly improved by the non-uniform magnetic field.

5. Conclusions

In the study, we presented the simulation of MNF saturated film boiling in presence of a non-uniform magnetic field. The effects of the non-uniform magnetic field on the heat transfer characteristics of a single-mode and multi-mode saturated film boiling of the MNF and the dynamics of phase interfaces were studied in detail under the constant wall temperature condition.

It is found that the departure diameter and time both decrease with an increase in the magnetic field intensity. Increasing magnetic field force in the vertical direction due to higher magnetic field intensity lead to the increase in the bubble velocity in the process of bubble formation, detachment and rise. And, when the magnetic field intensity continue to increases to a greater value, the bubble formation sites increase because of stronger interface instability.

It is easy to produce the instability phenomenon in multi-mode saturated film boiling as compared to single-mode film boiling. The instability becomes more intense when the magnetic field is applied. In a non-uniform magnetic field, as a result of the horizontal component of the magnetic field force, the instability wavelength of film boiling becomes shorter and the bubble formation sites on the heated wall gradually deviate towards the central axis during the bubble generation stage. With an increase in the magnetic field intensity, the deviation of the bubble increases due to the increasing horizontal component of the magnetic field force. When the magnetic field intensity increases further to higher value, the bubble formation and release loses its temporal periodicity and spatial asymmetry. The increased convection currents and vigorous disturbance of the flow field also lead to the lateral motion of bubbles on the central axis.

The heat transfer performance is enhanced with an increase in the magnetic field intensity in presence of non-uniform magnetic field. Particularly, the magnetic field has a greater influence on the film boiling for water near the critical pressure due to the dominant effect of the magnetic force.

Declaration of Competing Interest

The authors declared that there is no conflict of interest.

Acknowledgements

The authors acknowledge the support from the joint fund between the Chinese Academy of Sciences (CAS) and National Natural Science Foundation of China (NSFC) under the grant of U1738105.

References

[1] I. Nkurikiyimfura, Y. Wang, Z. Pan, Heat transfer enhancement by magnetic nanofluids—A review, Renew. Sustain. Energy Rev. 21 (2013) 548–561.
[2] M. Bahiraei, M. Hangi, Flow and heat transfer characteristics of magnetic nanofluids: A review, J. Magn. Magn. Mater. 374 (2015) 125–138.
[3] M.A. Khairul, E. Doroodchi, R. Azizian, B. Moghtaderi, Advanced applications of tunable ferrofluids in energy systems and energy harvesters: A critical review, Energy Convers. Manage. 149 (2017) 660–674.
[4] V.G. Bashtovoi, G. Challant, O.Y. Volkova, Boiling heat transfer in magnetic fluids, J. Magn. Magn. Mater. 122 (1993) 305–308.

[5] S. Kamiyama, J. Ishimoto, Boiling 2-phase flows of magnetic fluid in a nonuniform magnetic-field, J. Magn. Magn. Mater. 149 (1995) 125–131.
[6] S. Shuchi, T. Mori, H. Yamaguchi, Flow boiling heat transfer of binary mixed magnetic fluid, IEEE Trans. Magn. 38 (2002) 3234–3236.
[7] L. Xu, X.F. Peng, Fundamental analysis of boiling heat transfer of magnetic fluids in a magnetic field, Heat Transfer-Asian Res. 31 (2002) 69–75.
[8] J.H. Liu, J.M. Gu, Z.W. Lian, H. Liu, Experiments and mechanism analysis of pool boiling heat transfer enhancement with water-based magnetic fluid, Heat Mass Transf. 41 (2004) 170–175.
[9] S. Shuchi, K. Sakatani, H. Yamaguchi, Boiling heat transfer characteristics of binary magnetic fluid flow in a vertical circular pipe with a partly heated region, Proc. Instit. Mech. Eng. Part C-J. Mech. Eng. Sci. 218 (2004) 223–232.
[10] S. Shuchi, K. Sakatani, H. Yamaguchi, An application of a binary mixture of magnetic fluid for heat transport devices, J. Magn. Magn. Mater. 289 (2005) 257–259.
[11] J. Ishimoto, Stability of the boiling two-phase flow of a magnetic fluid, J. Appl. Mech. 74 (2007) 1187–1196.
[12] M.A. Kobozev, A.Y. Simonovskii, Formation rate of vapor bubbles in magnetic fluid boiling at a single vaporization center: Measuring technique and experimental setup, Tech. Phys. 52 (2007) 1422–1428.
[13] T. Lee, J.H. Lee, Y.H. Jeong, Pool boiling and flow boiling CHF enhancement at atmospheric pressure using magnetic nanofluid, in: 20th International Conference on Nuclear Engineering and the ASME 2012 Power Conference (ICONE20-POWER2012), Anaheim, CA, 2012, pp. 549–557.
[14] T. Lee, J.H. Lee, Y.H. Jeong, Flow boiling critical heat flux characteristics of magnetic nanofluid at atmospheric pressure and low mass flux conditions, Int. J. Heat Mass Transf. 56 (2013) 101–106.
[15] M. Şeşen, Y. Tekşen, B. Şahin, K. Şendur, M. Pınar Mengüç, A. Koşar, Boiling heat transfer enhancement of magnetically actuated nanofluids, Appl. Phys. Lett. 102 (2013).
[16] P. Naphon, Effect of magnetic fields on the boiling heat transfer characteristics of nanofluids, Int. J. Thermophys. 36 (2015) 2810–2819.
[17] A. Abdollahi, M. Reza Salimpour, Experimental investigation on the boiling heat transfer of nanofluids on a flat plate in the presence of a magnetic field, Eur. Phys. J. Plus 131 (2016).
[18] M. Shojaeian, M.M. Yildizhan, O. Coskun, E. Ozkalay, Y. Teksen, M.A. Gulgun, H. F.Y. Acar, A. Kosar, Investigation of change in surface morphology of heated surfaces upon pool boiling of magnetic fluids under magnetic actuation, Mater. Res. Express 3 (2016).
[19] A. Abdollahi, M.R. Salimpour, N. Etesami, Experimental analysis of magnetic field effect on the pool boiling heat transfer of a ferrofluid, Appl. Therm. Eng. 111 (2017) 1101–1110.
[20] R. Amirzehni, H. Aminfar, M. Mohammadpourfard, Experimental study of magnetic field effect on bubble lift-off diameter in sub-cooled flow boiling, Exp. Therm Fluid Sci. 89 (2017) 62–71.
[21] M.R. Özdemir, A.K. Sadaghiani, A.R. Motezakker, S.S. Parapari, H.S. Park, H.Y. Acar, A. Koşar, Experimental studies on ferrofluid pool boiling in the presence of external magnetic force, Appl. Therm. Eng. 139 (2018) 598–608.
[22] G. Karimi-Moghaddam, R.D. Gould, S. Bhattacharya, Investigation of enhancement in pool boiling heat transfer of a binary temperature sensitive magnetic fluid, in: ASME International Mechanical Engineering Congress and Exposition (IMECE2013), San Diego, CA, 2014.
[23] M. Mohammadpourfard, H. Aminfar, M. Sahraro, Numerical simulation of nucleate pool boiling on the horizontal surface for ferrofluid under the effect of non-uniform magnetic field, Heat Mass Transf. 50 (2014) 1167–1176.
[24] M. Mohammadpourfard, H. Aminfar, M. Karimi, Numerical investigation of non-uniform transverse magnetic field effects on the swirling flow boiling of magnetic nanofluid in annuli, Int. Commun. Heat Mass Transfer 75 (2016) 240–252.
[25] H. Aminfar, M. Mohammadpourfard, R. Maroofiazar, Numerical study of non-uniform magnetic fields effects on subcooled nanofluid flow boiling, Prog. Nucl. Energy 74 (2014) 232–241.
[26] A. Malvandi, Film boiling of magnetic nanofluids (MNFs) over a vertical plate in presence of a uniform variable-directional magnetic field, J. Magn. Magn. Mater. 406 (2016) 95–102.
[27] M.H. Taheri, M. Mohammadpourfard, A.K. Sadaghiani, A. Kosar, Wettability alterations and magnetic field effects on the nucleation of magnetic nanofluids: A molecular dynamics simulation, J. Mol. Liq. 260 (2018) 209–220.
[28] H. Ki, Level set method for two-phase incompressible flows under magnetic fields, Comput. Phys. Commun. 181 (2010) 999–1007.
[29] M.R. Ansari, A. Hadidi, M.E. Nimvari, Effect of a uniform magnetic field on dielectric two-phase bubbly flows using the level set method, J. Magn. Magn. Mater. 324 (2012) 4094–4101.
[30] D.X. Shi, Q.C. Bi, R.Q. Zhou, Numerical Simulation of a Falling Ferrofluid Droplet in a Uniform Magnetic Field by the VOSET Method, Numer. Heat Trans., Part A: Appl. 66 (2014) 144–164.
[31] K.K. Guo, H.X. Li, Y. Feng, T. Wang, J.F. Zhao, Numerical simulation of magnetic nanofluid (MNF) film boiling using the VOSET method in presence of a uniform magnetic field, Int. J. Heat Mass Transf. 134 (2019) 17–29.
[32] D.L. Sun, W.Q. Tao, A coupled volume-of-fluid and level set (VOSET) method for computing incompressible two-phase flows, Int. J. Heat Mass Transf. 53 (2010) 645–655.
[33] T. Wang, H.X. Li, Y.F. Zhang, W. Han, T.Y. Sheng, W.Q. Zhang, Numerical Simulation of Two-Phase Flows Using 3D-VOSET Method on Dynamically Adaptive Octree Grids, in: 2014 22nd International Conference on Nuclear Engineering, Prague, Czech Republic, 2014.
[34] J.U. Brackbill, D.B. Kothe, C. Zemach, A continuum method for modeling surface tension, J. Comput. Phys. 100 (1992) 335–354.
[35] R.E. Rosensweig, Ferrohydrodynamics, Cambridge University Press, Cambridge, 1985.
[36] K. Ling, G. Son, D.L. Sun, W.Q. Tao, Three dimensional numerical simulation on bubble growth and merger in microchannel boiling flow, Int. J. Therm. Sci. 98 (2015) 135–147.
[37] D.X. Shi, Investigation on Dynamic Behavior of Bubble and Ferrofluid Droplet under Magnetic Fields, in, Xi'an Jiaotong University, China, 2014.
[38] V.V. Klimenko, Film boiling on a horizontal plate — new correlation, Int. J. Heat Mass Transf. 24 (1981) 69–79.